PHYSICAL REVIEW D VOLUME 24, NUMBER 7 1 OCTOBER 1981

Photon structure via the Drell-Yan process

Jerome Busenitz and J. D. Sullivan
Department of Physics, University of Illinois at Urbana-Champaign, 1110 West Green Street, Urbana, Illinois 61801
(Received 1 June 1981)

We assess Drell-Yan photoproduction as a method of measuring the structure functions of the photon. The behavior of the cross section is examined in all variables: energy, lepton-pair rapidity, transverse momentum, and lepton-pair angular distribution. We also calculate the Bethe-Heitler background and examine the interference between the Drell-Yan and Bethe-Heitler amplitudes. We conclude that the Drell-Yan photoproduction cross section is probably too small in regions of interest to be observed in practical experiments even at Fermilab Tevatron energies.

I. INTRODUCTION

In this paper we explore Drell-Yan photoproduction, $\gamma N \to \mu^+\mu^- X$, as a means of determining the quark and gluon structure functions of the photon. Our work extends considerably that given in Ref. 1 (and also Refs. 2–4) by examining the full range of rapidity for the produced muon pair, the jet structure expected for final states, and also interference between the Bethe-Heitler and the Drell-Yan amplitudes. Unfortunately our conclusions are much the same as those reached in Ref. 1; namely, the Drell-Yan cross sections are extremely small in the regions of interest ($d^2\sigma/dQ^2dy \simeq 6\times 10^{-5}$ nb/GeV^2 at $Q^2=16$ GeV^2, $y=0$, and $s=300$ GeV^2) making experimental studies very difficult and perhaps impossible. As an aside we examine the possibility of using the Bethe-Heitler process itself as a probe of *target* structure functions.

The basic plan of our paper is as follows: In the remainder of this section we briefly review the special features of the photon structure functions which may be divided into pointlike and vector-dominance pieces. In Sec. II we discuss the jet topology which is predicted to be present in Drell-Yan photoproduction and in the Bethe-Heitler process. In Sec. III we present results for the fully differential $d^3\sigma/dQ^2dy\,dQ_\perp{}^2$ Drell-Yan cross section and also the once integrated $d^2\sigma/dQ^2dy$ cross section; in parallel we present the same quantities for the Bethe-Heitler background. Since the results presented in Sec. III correspond to integration over the *full angular phase space* of the final muons at fixed y, Q^2, and $Q_\perp{}^2$, there is no interference between the Drell-Yan and Bethe-Heitler contributions.

In Sec. IV we calculate the Drell-Yan–Bethe-Heitler interference contribution for certain restricted muon-angular-phase-space regions in order to investigate the possibility of using interference as a means of studying the quantum-chromodynamic (QCD) structure of the photon. In Sec. V we present our conclusions.

Photon structure functions

As first discussed by Witten[5] and further discussed and extended by other authors,[6–11] the parton structure functions of the photon differ in a dramatic way from those of hadrons. The asymptotic series in $\ln Q^2$ (equivalently the inverse running coupling constant) for the distribution function at scale Q^2 for finding a quark or gluon in the photon contains a leading term proportional to $\ln Q^2$, a next-to-leading term independent of $\ln Q^2$, and then a remainder having the familiar hadronic form of inverse powers of $\ln Q^2$. The first two terms, referred to as the pointlike part, dominate at large Q^2 and can be calculated without reference to hadronic structure. As the name implies, their presence is a consequence of the pointlike coupling of the photon to quarks. The remainders of the photon structure functions at scale Q^2 can be calculated only after input values at some $Q_0{}^2$ have been provided. These latter hadroniclike pieces are referred to as the vector-meson-dominance (VMD) contributions since the vector-dominance model

should provide a good guide to their size.

While all parts of the photon structure functions are interesting, the pointlike parts are especially so since they offer a very clean test of QCD. Among all the gauge particles which populate today's theories, only photons are available in laboratory beams. Even though it is universally expected that the $W^{\pm}$ and Z^0 will be produced as physical particles in the near future, beams of W's and Z's seem forever out of the question. Hence it is important to study the photon—the only laboratory gauge particle—by all possible means.

We write the distribution function for finding at scale Q^2 a quark or antiquark in the photon with flavor i and momentum fraction x as follows:

$$q_i^{\gamma}(x,Q^2)=\frac{\alpha}{2\pi}\left[f_i(x)\ln\left[\frac{Q^2}{\Lambda^2}\right]+s_i(x)\right]+q_i^{\mathrm{VMD}}(x,Q^2)\,, \tag{1.1}$$

where the index i denotes either charge $\pm\frac{2}{3}$ or charge $\pm\frac{1}{3}$. Similarly for the gluon distribtution we write

$$G^{\gamma}(x,Q^2)=\frac{\alpha}{2\pi}\left[f_G(x)\ln\left[\frac{Q^2}{\Lambda^2}\right]+s_G(x)\right]+G^{\mathrm{VMD}}(x,Q^2)\,. \tag{1.2}$$

The functions $f(x)$ and $s(x)$ are known from perturbative QCD calculations at the one-[5–9] and two-loop levels,[10,11] respectively. For our purposes high accuracy is not important. We use for the f's the simple analytic approximations given in Appendix A. We have chosen not to include the next-to-leading terms in our work even though simple expressions valid over much of the interval $0<x<1$ have been given by Bardeen and Buras.[10] We refer the reader to Ref. 10 for a discussion of the extent to which these next-to-leading-order contributions can be subsumed into the leading terms by an appropriate choice of the scale factor Λ. All results in Sec. III of this paper correspond to setting $s_i=s_G=0$, choosing $\Lambda=0.5$ GeV and four flavors: u, d, c, s.

For the vector-dominance contributions we assume

$$q_i^{\mathrm{VMD}}(x,Q^2)=\frac{4\pi\alpha}{f_V{}^2}q_i^{\rho}(x,Q^2) \tag{1.3}$$

with an *effective* coupling $f_V{}^2/4\pi=2.0$ and correspondingly for the gluon distribution. The current best value[12] for the photon-ρ coupling is $f_{\rho}{}^2/4\pi=2.2$. We use a slightly smaller effective coupling in order to include in an approximate manner the ω contribution. To see this note that $f_{\rho}{}^2/f_{\omega}{}^2=0.1$ from experiment and that $q_i^{\omega}(x,Q^2)\simeq q_i^{\rho}(x,Q^2)$ is a reasonable guess, at least for valence contributions. The net effect of higher-mass vector-meson contributions ϕ, ρ', ..., is likely to be no more than 20% if experience with other real-photon—initiated processes is a reliable guide. We estimate the ρ^0 distributions themselves with the help of the measurements of the $\pi^{\pm}$ distribution functions obtained from Drell-Yan productions in $\pi^{\pm}N$ collisions.[13,14] In particular our model has the properties that valence quarks in the ρ^0 carry 35% of the ρ^0 momentum and that the ρ^0 sea is SU(3) symmetric up to a value $Q_0=4$ GeV. Evaluation of the valence and sea structure functions beyond Q_0, including the development of a small charmed-quark contribution, is handled by the approximate method of Buras and Gaemers.[15] Such an approximation is more than adequate for our purposes. Details and explicit formulas for the vector-dominance pieces we use are spelled out in Appendix B. We have also treated the scale breaking of the target-proton structure functions by the method of Buras and Gaemers. The explicit formulas we use for the proton can be found in Ref. 15 and correspond to a $(1-x)^{10}$ gluon distribution.

In Sec. IV where we explore the size of the Drell-Yan—Bethe-Heitler interference term and its potential for exploitation, we have resorted to further approximation. Namely, in place of Eqs. (1.1) and (1.2) we use only the pointlike coupling of the photon to quarks evaluated without QCD radiative corrections and without smearing due to intrinsic transverse momentum. This is equivalent to the replacement of Eqs. (1.1) and (1.2) by

$$q_i^{\gamma}(x,\,Q^2)=\left[\frac{3\alpha}{2\pi}\right]\epsilon_i{}^2[x^2+(1-x)^2]\ln\left[\frac{Q^2}{m_i{}^2}\right]+O((\ln Q^2)^0)\,, \tag{1.4}$$

$$G^{\gamma}(x,Q^2)=0\,, \tag{1.5}$$

where $\epsilon_i{}^2=\frac{4}{9},\frac{1}{9}$ is the charge squared of quark (i), and $m_i{}^2$ is its mass. We refer to this as the *pointlike Born* contribution. A discussion of the accuracy of this approximation is saved for Sec. IV.

II. JET STRUCTURE

The final states of $\gamma N \to \mu^+\mu^- X$ at high energies and large-pair transverse momentum $Q_\perp$ have a jet structure which reveals the special role played by the photon in QCD. The situation closely parallels that for large-$p_\perp$ jet production via the $\gamma\gamma$ process in $e^\pm e^\pm$ collisions[6,16] and that for large-$p_\perp$ jet production[3,6,17,18] in real-photon–hadron collisions. This is to be expected since these latter two processes along with Drell-Yan photoproduction are alternative ways of measuring the photon structure functions.

Figure 1 shows the distinguishable contributions to Drell-Yan photoproduction at large $Q_\perp$. One has [Figs. 1(a)–1(d)] the three-jet events characteristic of any hadron-hadron Drell-Yan process and in addition as new contributions [Fig. 1(e)] two-jet events which are characterized by the absence of a spectator jet in the direction of the initial photon beam. These two-jet events are determined by the pointlike Born structure function [Eqs. (1.4) and (1.5)] and thus are particularly large in the $x \to 1$ limit. In Sec. III below we show separately the results for the two- and three-jet contributions to $d^3\sigma/dQ^2\,dy\,dQ_\perp{}^2$. As $Q_\perp$ is decreased to low values ($\sim 1-2$ GeV), spectator and large-transverse-momentum jets begin to overlap and continuously merge into an undifferentiated whole. The pointlike coupling of the photon still manifests itself but it is QCD radiatively corrected, Eqs. (1.1) and (1.2) and is therefore softer as $x \to 1$ than the Born structure function. At low $Q_\perp$ the effects of all the processes [Figs. 1(a)–1(e)] are included to leading-logarithmic accuracy in the basic Drell-Yan process, Fig. 1(f), when calculated with scale-broken structure functions.

The large-$Q_\perp$ jet structure of the Bethe-Heitler process is illustrated by Fig. 1(g). There are only two jets in the final state and no photon spectator jet. It is clear that this final state has the correct structure to interfere with the pointlike Born process of Fig. 1(e) and that the interference phase is known and fixed by QED. We study this interference in Sec. IV below.

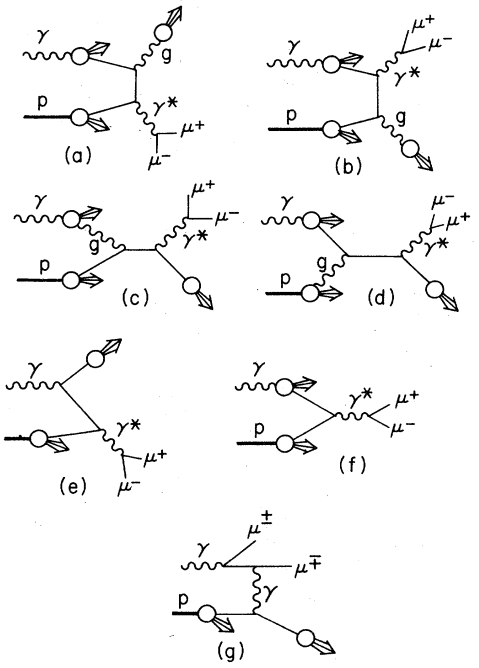

FIG. 1. Contributions to Drell-Yan production in photon beams; (a)–(d) three-jet contributions; (e) the two-jet contribution which has no photon-spectator jet; (f) the basic Drell-Yan process which at low $Q_\perp$ contains via scale-broken structure functions all of (a)–(e); (g) the Bethe-Heitler contribution which has the same two-jet topology as (e).

III. CROSS SECTIONS

Having reviewed the special features of the photon structure functions and the jet topologies which they imply, we now present Drell-Yan differential cross sections at energies appropriate to Fermilab and CERN SPS as well as future operations at Fermilab Tevatron. In parallel with the Drell-Yan cross section, we show the Bethe-Heitler cross section since the latter is an unavoidable background. All results shown in this section correspond to integration over all angular regions of the μ^+ (and μ^-) in the $\mu^+\mu^-$ rest frame; hence there is no interference between the Drell-Yan and Bethe-Heitler contributions. Kinematic variables are defined in Fig. 2.

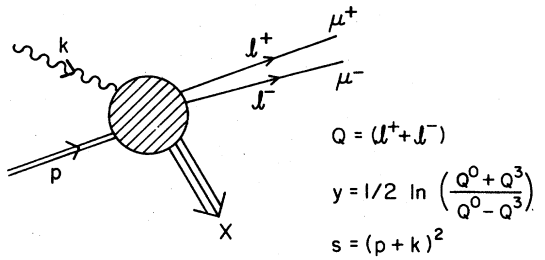

FIG. 2. Kinematic variables used to specify the Drell-Yan process. The rapidity y refers to the overall center-of-mass system in which the incident real photon moves in the positive z direction.

A. Formulas

We give results for $d^2\sigma/dQ^2dy$ as well as $d^3\sigma/dQ^2dy\,dQ_\perp{}^2$ where for the latter we concentrate on the low-$Q_\perp$ region in which the cross section is largest. As discussed in Sec. II the unique jet structure is not revealed until one goes to large $Q_\perp$ values. The cross-section formulas we use are the well-known expression of Drell and Yan,[19]

$$\frac{d^2\sigma^{\mathrm{DY}}}{dQ^2\,dy}=\frac{4\pi}{9}\frac{\alpha^2}{Q^2s}\sum_{i=1}^{2f}\epsilon_i{}^2[q_i^\gamma(\sqrt{\tau}e^y,Q^2)\times q_i^p(\sqrt{\tau}e^{-y},Q^2)]\,, \tag{3.1}$$

and, for the cross section differential in $Q_\perp$, the prescription of Altarelli, Parisi, and Petronzio[20],

$$\frac{d^3\sigma^{\mathrm{DY}}}{dQ^2dy\,dQ_\perp{}^2}=\frac{d^2\sigma^{\mathrm{DY}}}{dQ^2dy}f(Q_\perp{}^2)+\frac{1}{\pi}\int d^2k_\perp\frac{d\tilde{\sigma}}{dQ^2dy\,dk_\perp{}^2}[f((Q_\perp-k_\perp)^2)-f(Q_\perp{}^2)]\,, \tag{3.2}$$

where

$$f(Q_\perp{}^2)=Ae^{-AQ_\perp{}^2} \tag{3.3}$$

and[20,21]

$$\frac{d\tilde{\sigma}}{dQ^2dy\,dk_\perp{}^2}=\frac{\alpha^2\alpha_S(Q^2)}{Q^2s^2}\sum_{i=1}^{2f}\epsilon_i{}^2\int dx_1dx_2\delta(x_1x_2-\tfrac{1}{2}x_1\bar{x}_\perp e^{-y}-\tfrac{1}{2}x_2\bar{x}_\perp e^{y}+\tau)$$
$$\times[q_i^\gamma(x_1,Q^2)q_i^p(x_2,Q^2)F_{q\bar{q}}(x_1x_2,\tau,x_\perp)+q_i^\gamma(x_1,Q^2)G^p(x_2,Q^2)F_{qG}(x_1,x_2,\tau,x_\perp,y)$$
$$+G^\gamma(x_1,Q^2)q_i^p(x_2,Q^2)F_{qG}(x_2,x_1,\tau,x_\perp,-y)] \tag{3.4}$$

with

$$F_{q\bar{q}}(x_1x_2,\tau,x_\perp)=\frac{32}{27x_\perp{}^2}\left[1-\frac{x_\perp{}^2}{2x_1x_2}+\frac{\tau^2}{(x_1x_2)^2}\right], \tag{3.5}$$

$$F_{qG}(x_1,x_2,\tau,x_\perp,y)=\frac{1}{9(x_1x_2)^2}\left[\frac{x_1{}^2\bar{x}_\perp{}^{-2}e^{-2y}+4(x_1x_2-\tau)^2}{2x_1\bar{x}_\perp e^{-y}-4\tau}\right]. \tag{3.6}$$

In Eqs. (3.1)–(3.6) the sums run over f flavors of quarks and f flavors of antiquarks, ϵ_i is the quark fractional charge, $\tau=Q^2/s$, $x_\perp=2k_\perp/\sqrt{s}$, $\bar{x}_\perp=(4\tau+x_\perp{}^2)^{1/2}$, $\alpha_S(Q^2)=12\pi/[(33-2f)\ln(Q^2/\Lambda^2)]$, and all quark masses have been set equal to zero. We take $f=4$ and $\Lambda=0.5$ GeV throughout.

Equation (3.2) is an interpolation between the low-$Q_\perp$ region where parton intrinsic transverse momentum — represented by the function $f(Q_\perp{}^2)$— is important and the region of large $Q_\perp$ where the muon-pair transverse momentum is balanced by a single quark or gluon jet and can be reliably calculated in QCD from Eq. (3.4) alone ($k_\perp\to Q_\perp$). Although Eq. (3.2) does not have a fundamental basis it represents pN data well and appears to be a reasonable prescription for cutting off the $k_\perp\to 0$ divergent (and obviously wrong) behavior of the first-order QCD expression (3.4). The appropriate value of the parameter A which describes the joint effect of parton transverse momenta in the target and beam, is somewhat uncertain. We use $A=1.3$ GeV^{-2} which fits pN Drell-Yan (DY) production well.[20] We find $\lesssim 25\%$ changes in our results over the interval $0<Q_\perp<2.0$ GeV when we vary A over the range 1.0 and 1.6 GeV^{-2}. We calculate the Bethe-Heitler (BH) cross section from[1]

$$\frac{d^3\sigma^{\mathrm{BH}}}{dQ^2dy\,dQ_\perp{}^2}=\frac{\alpha^3}{2p\cdot(k-Q)}\left[\sum_{i=1}^{2f}\epsilon_i{}^2q_i^p(x,-\bar{t})\right]\frac{(Q^2-4m_\mu{}^2)^{1/2}}{\bar{t}\,\bar{s}Q(Q^2-\bar{t})^2}\left[(B_1+B_2)-\frac{2\bar{s}\bar{u}}{(Q^2-\bar{t})^2}(B_1+3B_2)\right], \tag{3.7}$$

where

$$B_1=2(Q^4+\bar{t}^2)+8Q^2m_\mu{}^2+\frac{-2Q}{(Q^2-4m_\mu{}^2)^{1/2}}[2(Q^4+\bar{t}^2)+m_\mu{}^2(8Q^2-8\bar{t}-16m_\mu{}^2)]\ln\left[\frac{Q+(Q^2-4m_\mu{}^2)^{1/2}}{2m_\mu}\right] \tag{3.8}$$

and

$$B_2=4Q^2\bar{t}-\frac{16m_\mu{}^2\bar{t}Q}{(Q^2-4m_\mu{}^2)^{1/2}}\ln\left[\frac{Q+(Q^2-4m_\mu{}^2)^{1/2}}{2m_\mu}\right] . \tag{3.9}$$

In the above, the subprocess Mandelstam variables are

$$\begin{aligned}\bar{s}&=(k+xp)^2\simeq xs ,\\ \bar{t}&=(Q-k)^2\simeq s(\tau-\tfrac{1}{2}\bar{x}_\perp e^{-y}) ,\\ \bar{u}&=(Q-xp)^2\cong s(\tau-\tfrac{1}{2}x\bar{x}_\perp e^{y}) ,\end{aligned} \tag{3.10}$$

and, in addition,

$$\begin{aligned}2p\cdot(k-Q)&=s(1-\tfrac{1}{2}\bar{x}_\perp e^{y}) ,\\ x&=(\tau-\tfrac{1}{2}\bar{x}_\perp e^{-y})/(1-\tfrac{1}{2}\bar{x}_\perp e^{y}) .\end{aligned} \tag{3.11}$$

To determine $d^2\sigma^{\rm BH}/dQ^2dy$ we integrate Eq. (3.7) numerically over the physically allowed region of $Q_\perp$ for fixed s, Q^2, y. Equation (3.7) is a parton-model approximation to the exact Bethe-Heitler cross section and is valid in the deep-inelastic region which is roughly defined by $|\bar{t}|>1$ GeV^2. It is not necessary to develop a formula for smaller values of $|\bar{t}|$ since in such regions the BH cross section overwhelms the DY cross section in every case. At the end of this section we show the effect of making $\bar{t}$ cuts on the BH cross section. We need not consider the elastic BH contribution.

A more sophisticated calculation of the Bethe-Heitler cross section would take into account the intrinsic transverse momentum of the target quark. In the spirit of Eq. (3.2) we write

$$\frac{d^3\sigma^{\rm BH}}{dQ^2dy\,dQ_\perp{}^2}=\frac{1}{\pi}\int d^2k_\perp g((\vec{k}_\perp-\vec{Q}_\perp)^2)\frac{d\tilde{\sigma}^{\rm BH}}{dQ^2dy\,dk_\perp{}^2} , \tag{3.12}$$

where

$$g(Q_\perp{}^2)=Be^{-BQ_\perp{}^2}$$

and $d\tilde{\sigma}^{\rm BH}/dQ^2dy\,dk_\perp{}^2$ is given by Eq. (3.7) with $Q_\perp$ replaced by $k_\perp$. Since only target effects are present in the Bethe-Heitler process, in contrast to combined target and beam effects in the Drell-Yan process, we take $B=2A$ in our calculations. However, because the cross section (3.7) is not divergent as $k_\perp\to 0$ and because the BH amplitude has a rather flat dependence on $k_\perp$ over the Q^2 range of interest, Eq. (3.12) differs numerically from Eq. (3.7) by no more than 5%. Thus Eq. (3.7) alone is adequate for our purposes.

We have checked our BH results against the results of an algebraic computer evaluation of the Feynman trace and against the formulas of Tsai.[22] We have also checked against the BH curves shown in Refs. 3 and 4 and find good agreement when allowance is made for small differences in structure functions.

B. Results

Figure 3 shows the pair-production cross section integrated over $Q_\perp$ for $s=300$ GeV^2, a typical Fermilab or CERN SPS value, and $y=0$ as a function of pair mass squared Q^2. Figure 4 shows the same at $s=1200$ GeV^2, a value appropriate to Fermilab Tevatron energies. One notes that although the Drell-Yan contribution exceeds the Bethe-Heitler background up to $Q\simeq 7.0$ GeV, the "signal-to-noise" ratio is never as large as a factor of 10 for $Q\gtrsim 3$ GeV at $s=300$ GeV^2. (Results from hadron-hadron experiments show that $Q\simeq 3$ GeV is roughly the lower limit of applicablility of the Drell-Yan model.) For the higher s value of Fig. 4 the situation is somewhat better; the BH contribution is less than 10% of the DY over $3\lesssim Q\lesssim 5$ GeV and remains less than 20% up to $Q\simeq 6.5$ GeV.

The DY and BH cross sections have very different dependences on y, the pair center-of-mass rapidity. This is shown in Figs. 5 and 6 for $Q=4.0$ and 7.5 GeV, respectively. The BH cross section

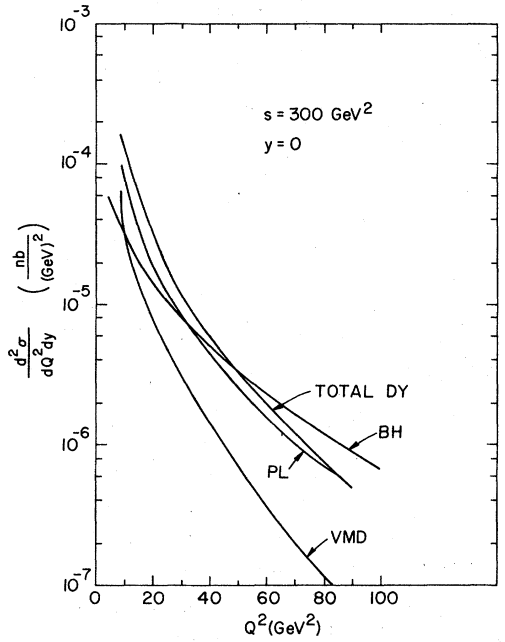

FIG. 3. The Drell-Yan and Bethe-Heitler cross sections integrated over $Q_\perp$ at $s=300$ GeV^2 and $y=0$. The curve labeled "total DY" is the sum of the vector-meson-dominance (VMD) and QCD-corrected pointlike (PL) contributions.

is sharply peaked foward in y as expected; the DY is rather flat in y except near the kinematic end points. It is clear that going to negative values of y brings about significant improvements in the

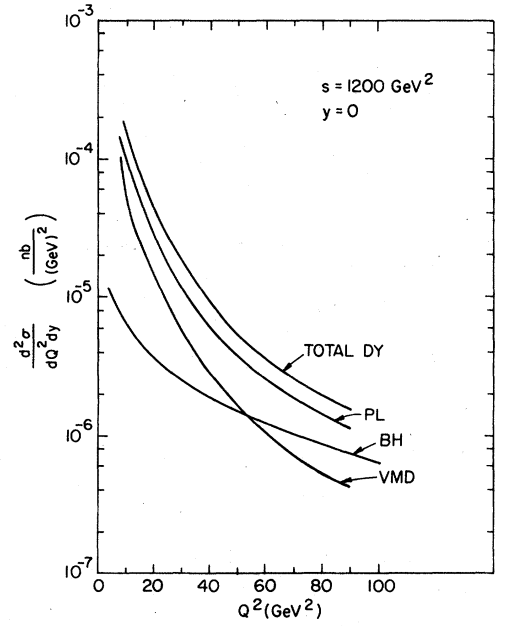

FIG. 4. Same as Fig. 3 except at $s=1200$ GeV^2.

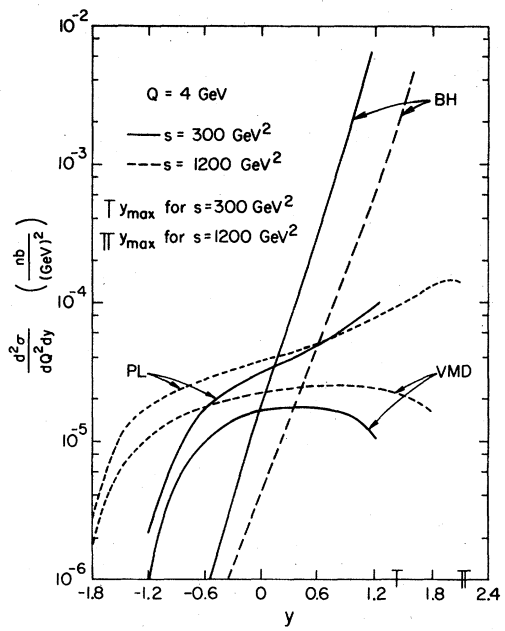

FIG. 5. The rapidity dependences of the vector-meson-dominance (VMD) and QCD-corrected pointlike (PL) contributions to Drell-Yan production at $Q=4$ GeV and the associated Bethe-Heitler (BH) background at two different center-of-mass energies. The kinematic limit in rapidity is indicated on the horizontal axis and corresponds to $x_1 \cong 1$, where x_1 is the argument of the photon structure function.

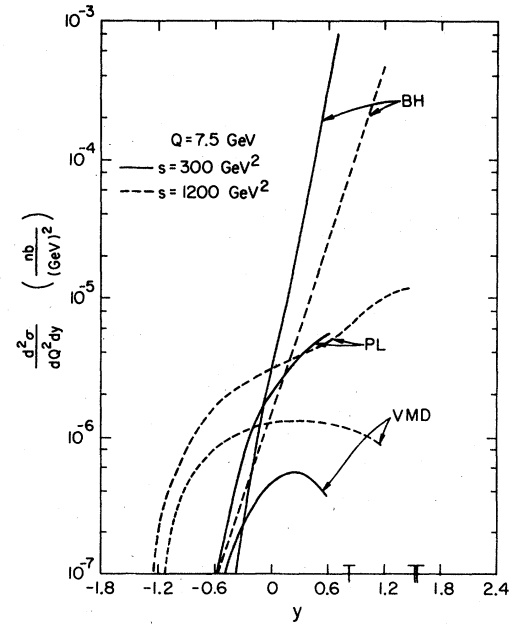

FIG. 6. Same as Fig. 5 except at $Q=7.5$ GeV.

signal-to-noise ratio while sacrificing only a factor of 2 or less in DY signal strength. The DY cross section is nowhere large, however.

In Figs. 7 and 8 we show the fully differential cross section as a function of y for $Q=4.0$ GeV, $Q_\perp=0.8$ GeV, and our two standard s values. The same features observed in Figs. 5 and 6 obtain; namely, for negative values of y the BH/DY ratio is less than 1/10. The curves labeled "Born PL" correspond to the two-jet contribution and will be discussed further in Sec. IV below.

We note for the cases shown in Figs. 3–8 the pointlike contribution to the DY cross section exceeds the vector-dominance contribution by less than a factor of 10 over the entire range in which the total DY cross section is longer than the BH cross section. There are regions outside that range where the pointlike contribution dominates the vector-dominance contribution, but in every case the Bethe-Heitler background is overwhelming. Unfortunately then, a clean study of the particularly interesting pointlike contribution appears impossible.

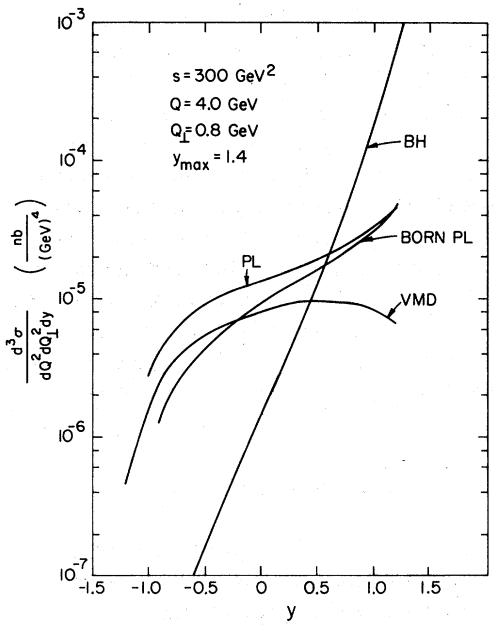

FIG. 7. The fully differential Drell-Yan and Bethe-Heitler cross sections at $Q=4.0$ GeV, $Q_\perp=0.8$ GeV, and $s=300$ GeV^2 as a function of rapidity. The curve labeled "Born PL" corresponds to the two-jet contribution and at *large* $Q_\perp$ is an additional contribution to the Drell-Yan cross section. At the low value of $Q_\perp$ chosen for this plot direct addition of the two pointlike contributions would involve substantial double counting as discussed in the text.

In Figs. 9 and 10 we show the full differential cross sections as a function of $Q_\perp$ for $Q=4$ GeV and $y=-0.6$ at two s values. Results for other values of Q and/or y can be approximated by interpolating from the information shown in Figs. 3–10. We note the favorable feature that the DY contribution is more sharply peaked in the low-$Q_\perp$ region than the BH contribution. In particular the region $0<Q_\perp<3$ GeV at $s=300$ GeV^2 and an even wider region at $s=1200$ GeV provides a comfortable DY/BY margin. Unfortunately the DY cross section is depressingly small at either s value. Note that the Born pointlike contribution dominates at large $Q_\perp$ as expected.

In an attempt to find some kinematic region with a larger cross section we show in Fig. 11 the results for a very low value of the pair mass, $Q=2$ GeV. We have also picked a reduced value, $s=100$ GeV^2, since secondary photon beam fluxes will typically be larger at lower photon energies. We see values $d^3\sigma/dQ^2dQ_\perp{}^2dy \gtrsim 10^{-4}$ nb/GeV^4 over a modest range of y at $Q_\perp=0.8$ GeV. The behavior as a function of $Q_\perp$ can be crudely guessed by using the simple exponential factor Eq. (3.3). We save for Sec. V a discussion of the feasibility of detecting the Drell-Yan cross section at any energy.

We see from Figs. 5–8 that for small values of $(y_{\max}-y)$ the BH cross section grows to quite large values. Is this large Bethe-Heitler cross sec-

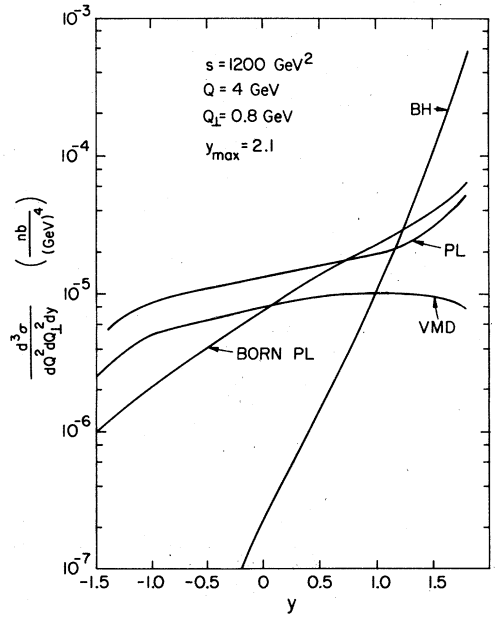

FIG. 8. Same as Fig. 7 except at $s=1200$ GeV^2.

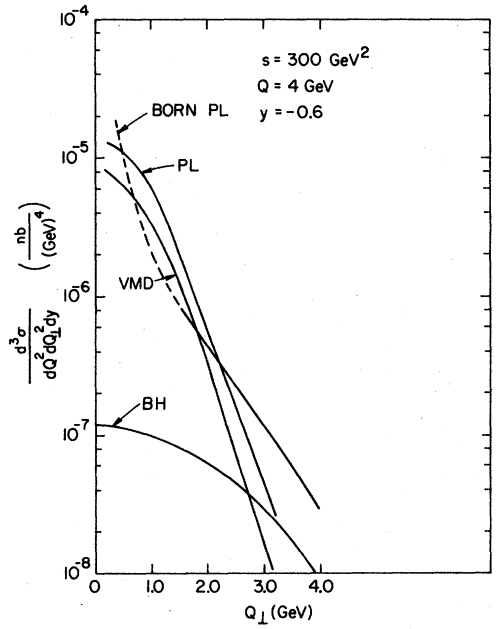

FIG. 9. The fully differential Drell-Yan and Bethe-Heitler cross sections as a function of $Q_\perp$ at $Q=4$ GeV, $s=300$ GeV^2, and $y=-0.6$. For $Q_\perp \gtrsim 1.5$ GeV the total Drell-Yan cross section is the sum of the VMD, PL, and Born PL contributions. As expected the Born pointlike contribution dominates at large $Q_\perp$. At values $Q_\perp \lesssim 1.0$ GeV the Drell-Yan cross section is given entirely by the PL and VMD pieces adding the Born PL in this region would involve double counting. The region 1.0 GeV $\lesssim Q_\perp \lesssim 1.5$ GeV is intermediate in character.

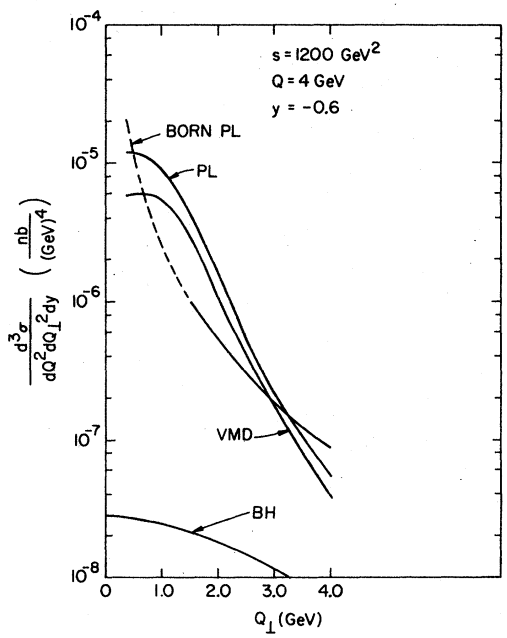

FIG. 10. Same as Fig. 9 except at $s=1200$ GeV^2 in character.

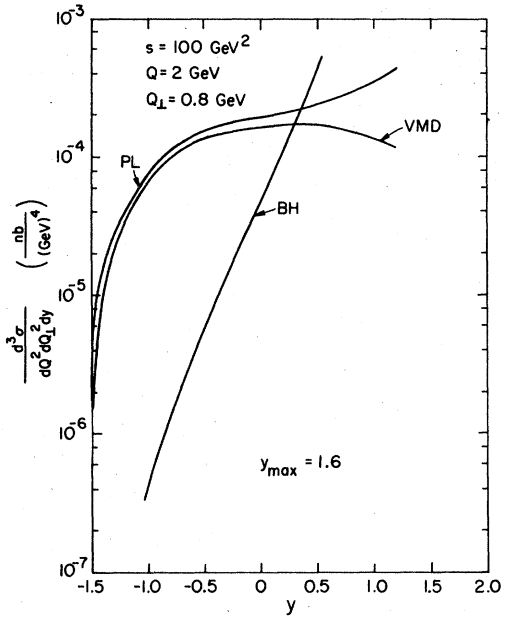

FIG. 11. Same as Fig. 7 except at a low pair mass, $Q=2$ GeV, and a low center-of-mass energy.

tion of interest? We believe the answer is *no* since the large cross-section values are simply a consequence of the photon-propagator enhancement of the BH diagrams at low $|\bar{t}|$. This is illustrated in Table I where the BH cross section is given for a few values of $\bar{t}$ and Q. In the table, values of y have been chosen close to y_{max} and hence vary with Q and s. We see that the BH cross section takes a precipitous decline whenever one asks that $-\bar{t}$ be large. Clearly, this method of probing the target-proton structure with virtual photons (mass$^2=\bar{t}$) is no competition for the conventional deep-inelastic lepton-scattering experiments.

IV. INTERFERENCE

The Drell-Yan—Bethe-Heitler interference contribution is of interest because it is proportional to the third power of the participating quark charge in contrast to the fourth power for the Drell-Yan process and the second power in deep-inelastic scattering. In addition, the fact that there are kinematic regions where the Bethe-Heitler amplitude is large admits the possibility of observing a small Drell-Yan amplitude directly by interference with the Bethe-Heitler amplitude in much the same way that one measures the phase of the strong interaction contribution to an elastic-scattering am-

TABLE I. The Bethe-Heitler cross section on protons at selected values of $-\bar{t}$.

s (GeV^2)	Q^2 (GeV^2)	$-\bar{t}$ (GeV^2)[a]	x	y	$d^2\sigma^{BH}/dQ^2dQ_\perp{}^2dy$ (nb/GeV^4) at $Q_\perp=0.8$ GeV
300	16.00	1.33	0.115	1.40	0.50×10^{-1}
300	56.25	2.35	0.287	0.80	0.28×10^{-2}
300	121.00	1.61	0.740	0.44	0.68×10^{-3}
750	16.00	1.33	0.042	1.86	0.58×10^{-1}
750	56.25	2.34	0.113	1.26	0.34×10^{-2}
750	121.00	1.55	0.303	0.90	0.43×10^{-2}
1200	16.00	1.33	0.024	2.10	0.66×10^{-1}
1200	56.25	2.33	0.069	1.49	0.35×10^{-2}
1200	121.00	1.54	0.189	1.14	0.53×10^{-2}

[a]For $-\bar{t}\lesssim1.8$ GeV^2 quark distribution functions evaluated at scale $-\bar{t}=1.8$ GeV^2 are used.

plitude in the forward direction by interference with Coulomb amplitude.

Motivated by the above considerations we investigate in this section the size of the DY-BH interference contribution (INT) to the $\gamma+p\to\mu^+\mu^-+X$ cross section. As mentioned earlier this interference is observable only if one integrates over regions of muon phase space which are *not* symmetric under interchange of the μ^+ and μ^-. Since our purposes are exploratory, it is not necessary to use a model as detailed as that used in Sec. III. Rather we use a simplified model which is defined by the Feynman diagrams in Fig. 12. We note that this model is exact for the BH contribution but approximate for the DY process. For the latter process we include the pointlike photon-quark coupling while ignoring the accompanying QCD radiative corrections and the vector-dominance contribution. As shown by the curves labeled BORN PL in Figs. 7–10 this approximation to the DY cross section is a good representation of the $Q_\perp$ and y behavior of the more refined model defined by Eqs. (3.1) and (3.2) except in the region of very low transverse momenta $Q_\perp\lesssim0.5$ GeV. (As discussed in Sec. II in the region of very large $Q_\perp$ the Born model becomes dominant for the DY amplitude. However, this latter region plays little role in our considerations here.) In addition to using the simplified amplitude defined in Fig. 12 we also neglect in this section scale-breaking contributions to the quark distribution functions of the proton target. In part for historic reasons and in part to explore the sensitivity to the choice of structure functions we use in this section the structure functions (without charm) given by Fox[23] with slight modifications; see Eq. (6) of Ref. 1 for explicit formulas. In addition we set the quark mass everywhere equal to 0.5 GeV. Since in the end we will extract from our calculations only *ratios* of the interference cross section to the DY or BH cross section, we believe that our simplified model is more than adequate to the exploratory task at hand and that our results are accurate to $\pm25\%$ for such ratios.

The traces encountered in calculating the BH, DY, and INT contributions from the diagrams of Fig. 12 were evaluated with the help of the algebraic program ASHMEDAI.[24] Next an integration over a restricted region of muon phase space was

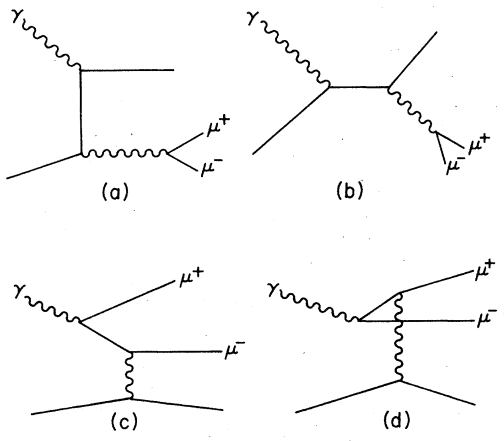

FIG. 12. The Born pointlike diagrams (a),(b) which are used along with the Bethe-Heitler diagrams (c), (d) to calculate the interference between the DY and BH amplitudes.

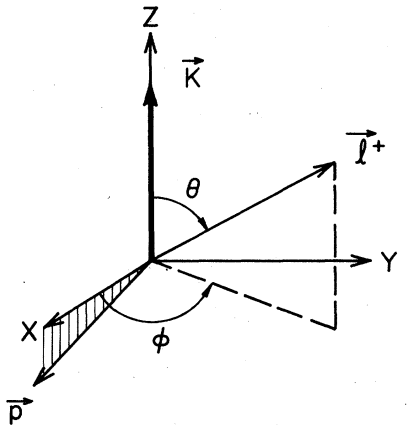

FIG. 13. The coordinate system we use to specify the orientation (θ,ϕ) of the three-momentum of the μ^+ in the $\mu^+\mu^-$ center-of-mass system. The incoming photon as viewed in this frame defines the z axis, and the xz plane is defined so as to contain the target-nucleon three-momentum.

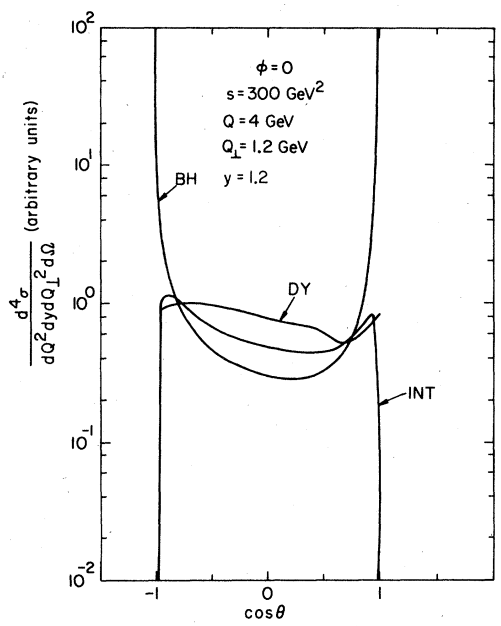

FIG. 14. Contributions to the muon-pair cross section differential in solid angle at $\phi=0$ as a function of θ. BH is the Bethe-Heitler contribution, DY is the Drell-Yan contribution calculated in the pointlike Born approximation, and INT is the contribution coming from Bethe-Heitler–Drell-Yan interference. For plotting convenience each contribution has been normalized to unity at $\cos\theta=-0.8$. To get the sizes of the BH and INT contributions relative to the DY contribution, multiply the BH contribution by 41.0 and the INT contribution by 6.3.

done by hand (analytically) and then the resulting expression evaluated numerically by a computer program to give the cross-section values. We have checked the results of this procedure for the DY and BH pieces against Sec. III formulas for the special case of integrating over the full muon phase space. In addition in order to verify our results for the interference contribution, we have written a separate computer program which evaluates the traces of Fig. 12 *numerically* for a given kinematical configuration and then integrates numerically over a prescribed region of muon phase space.

For given value of s and fixed Q^2, $Q_\perp$, and y, the muon phase space can be specified by angular parameters. We work in the pair center-of-mass frame $\vec{Q}=0$, choose coordinate axes as defined in Fig. 13, and specify the pair configuration by spherical angles θ and ϕ for the *positive* muon; the full phase space corresponds to $-1\leq\cos\theta\leq+1$ and $-\pi\leq\phi\leq+\pi$. Under the interchange $\theta\to\pi-\theta$ and $\phi\to\phi+\pi$ the BH and DY cross sections are invariant; INT changes sign.

The shapes of the various terms in the cross section as a function of θ and ϕ are shown in Figs. 14 and 15, respectively, for $s=300$ GeV^2, $Q=4$ GeV, $Q_\perp=1.2$ GeV, and $y=1.2$. For values of y in this region the shapes are practically independent of s, Q^2, and $Q_\perp$. Note that the relative sizes of the various contributions cannot be read from Figs. 14 and 15 since for plotting purposes each separate contribution has been normalized to unity at a convenient point (see figure captions).

One notes that much of the contributions to the BH cross section come from the end-point regions $\cos\theta=\pm1$ corresponding to the near vanishing of the muon propagator in either the first or second BH diagram in Fig. 12. It is clear that a substantial BH/DY suppression could be achieved independent of interference considerations by cutting out the regions near $\cos\theta=\pm1$. We also see that the sign of the interference contribution is positive in the hemisphere $-1\lesssim\cos\theta\lesssim1$, $-\pi/2\lesssim\phi\lesssim\pi/2$ and negative in the opposite hemisphere. Hence integration over the full range of ϕ at any fixed θ will typically lead to a small net contribution from INT.

In Figs. 16 and 17 we show separately the three contributions to the differential cross section for $s=300$ GeV^2, $Q=4$ GeV vs $Q_\perp$ (Fig. 16) and vs y (Fig. 17) for integration over a hemisphere in the muon phase space chosen to maximize the interference contribution. We also show in Fig. 17 the effect of excluding the end-point regions

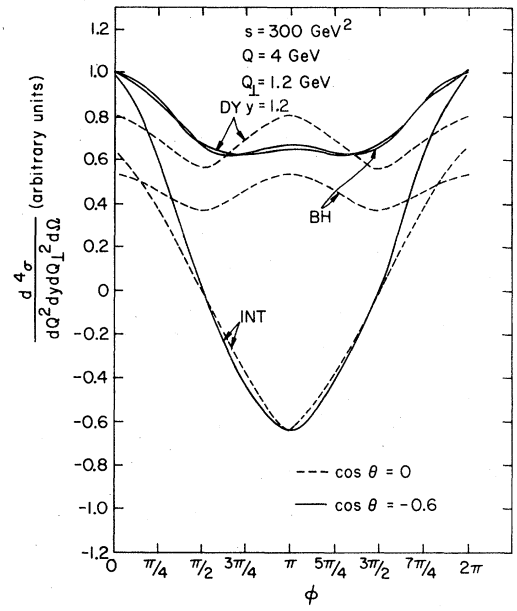

FIG. 15. Same as Fig. 14 except as a function of ϕ at fixed θ. Again, for convenience, each contribution has been normalized to unity at $\phi=0$ and $\cos\theta=-0.6$. The dashed lines correspond to $\cos\theta=0$ and the solid to $\cos\theta=-0.6$. Multiplying the BH and INT contributions by 23.6 and 4.8, respectively, yields their sizes relative to the DY contribution.

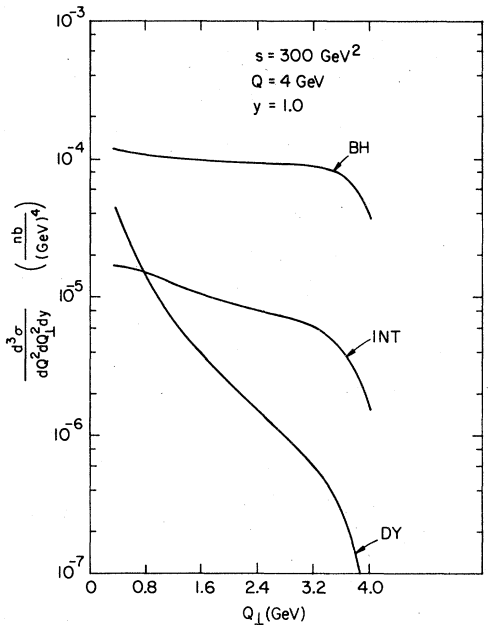

FIG. 16. Contributions to the muon-pair cross section as a function of $Q_\perp$ after integrating over the hemisphere $-1\le\cos\theta\le 1$, $-\pi/2\le\phi\le\pi/2$ of the μ^+ phase space.

$0.9<|\cos\theta|<1.0$ from the allowed region. In Fig. 18 we show corresponding information for the cross-section contributions integrated over $Q_\perp$ in the region where INT is at least one-tenth of BH.

We see from Fig. 16 that the cross-section ratio INT/BH is less than 15% at $y=1.0$ over almost the full range of $Q_\perp$ shown. The INT contribution is small on an absolute scale as well. We learn from Figs. 17 and 18 that in the very forward region $y\simeq 1.3$ where the BH differential cross section rises to $\sim 10^{-3}$ nb/GeV^2 the INT contribution, although larger than at smaller y, remains only $a\sim 10\%$ fraction BH. A general trend is clear from the figures; as one moves forward in y, all contributions increase but the ratio INT/BH is a decreasing function. Since it is hard to imagine that one could achieve better than a 10% experimental accuracy in such a muon-pair experiment, we conclude that looking for the INT contribution in a Bethe-Heitler dominated region of muon pair production is not practical. We learn another useful piece of information as well. In an experiment searching directly for the Drell-Yan contribution as explored in Sec. III, DY-BH interference effects due to asymmetric experimental acceptances, etc.,

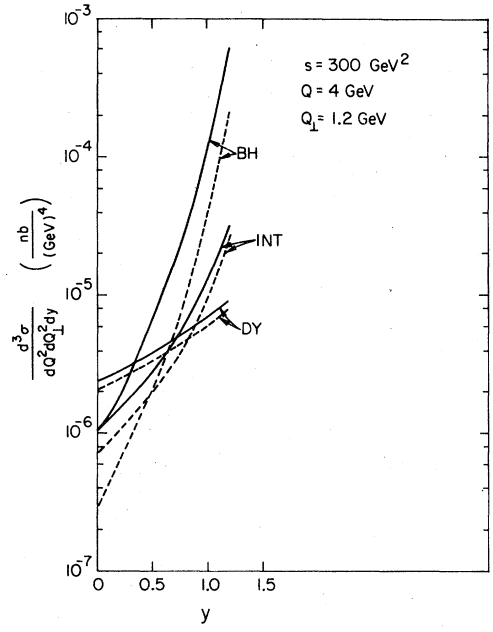

FIG. 17. Same as Fig. 16, except as a function of rapidity y at fixed $Q_\perp$. The additional set of dashed curves shows the effect of excluding the end-point regions $0.9<|\cos\theta|\le 1$ in which BH amplitude is especially large.

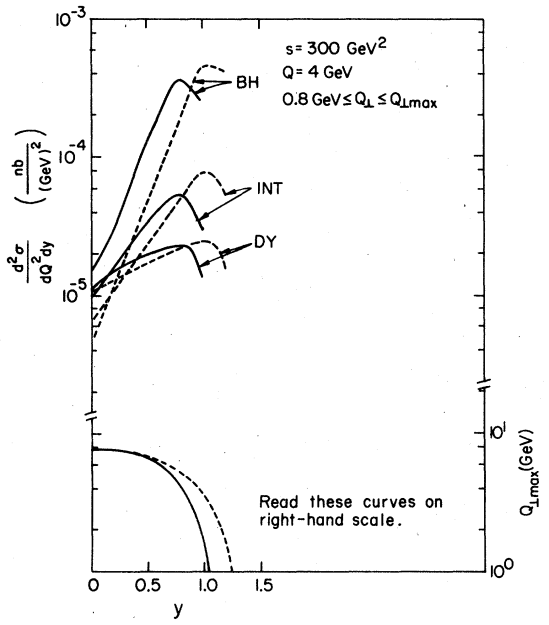

FIG. 18. The three contributions to the muon-pair cross section after integrating over transverse momentum $Q_\perp$ from 0.8 GeV to $Q_{\perp\,\max}$, the value of $Q_\perp$ at which the ratio INT/BH drops to 0.1. The solid and dashed curves refer to the same regions of μ^+ angular phase space as those in Fig. 17. The insert at the bottom of the figure shows the variation of $Q_{\perp\,\max}$ with y for the two cases.

are probably very small. One can, moreover, cut out the regions $|\cos\theta| \sim 1$ and further enhance the DY/BH ratio in such experiments.

V. SUMMARY AND EXPERIMENTAL OUTLOOK

In the previous sections we examined the cross section for Drell-Yan photoproduction as a function of energy and the several variables which are required to specify the lepton pair in the final state. As we found, there are large regions of phase space where the DY cross section dominates the BH background. Given the small size of the DY cross section, however, one must ask if in fact Drell-Yan photoproduction is a practical experiment.

To answer this we first note (see also various figures in Ref. 1) that for small pair masses, rapidities in the central region and low transverse momenta, the Drell-Yan cross section is weakly dependent on photon beam energy. This means that one has the option using either tagged photon beams or broad-band photon beams. Since it seems inevitable that greater fluxes can be obtained with broad-band beams, we concentrate entirely on this latter case.

As a model photon beam we take[25]

$$\frac{dM_{12}}{dk} = (3.5\times 10^5)\left[\frac{E}{400}\right]^2 \exp\left[-\left[\frac{400}{E}\right]0.021k\right], \tag{5.1}$$

where E is the energy in GeV of the primary protons which strike the photon production target, $k \simeq s/2m_p$ is the energy in GeV of the produced photons (mostly from π^0 decays), and M_{12} is the number of such photons in the secondary beam *per* 10^{12} *primary protons* on target. The above expression fits well the 25 GeV $\leq k \leq 0.75E$ spectrum of the broad-band beam used in the 87A-401 series of experiments carried out at Fermilab. It includes the reduction in photon yield caused by the filter which is required to suppress the large neutral-hadron (predominantly neutron) contamination which would otherwise be present in the photon beam. We note from Eq. (5.1) that the photon yield at *fixed* k increases faster than E^2 because of the exponential factor. Hence, the highest primary proton energies are desirable; we choose $E = 1$ TeV.

We choose a 0.1-radiation-length target; longer targets would increase the DY yield somewhat but would greatly increase the BH e^+e^- backgrounds and thereby swamp the detection apparatus. Thus $N_{\rm DY}$, the number of DY counts recorded in the course of the experiment, can be written

$$\frac{d^2N^{\rm DY}}{dQ^2dy} = \int dk \left[\frac{N_p}{10^{12}}\right]\frac{dM_{12}}{dk}(0.1L\rho)\left[\frac{d^2\sigma^{\rm DY}}{dQ^2dy}\right]\epsilon, \tag{5.2}$$

where N_p is the total number of protons on target, L is the radiation length of the target material, ρ is nucleon number density, and ϵ the detector efficiency. We choose liquid deuterium, $L\rho = 7.5\times 10^{25}$ cm^2, since it seems to offer the best combination of low Z and high nucleon density. Taking $N_p = 8.6\times 10^{17}$ which corresponds to 60 days of 1-TeV protons delivered at an average rate of 1×10^{13} protons/min, $\epsilon = 1$, and neglecting any difference between proton and neutron cross sections, we find the numbers given in Table II.

The yields are depressingly small. We conclude that Drell-Yan photoproduction in interesting regions is not measurable even at Fermilab Tevatron unless much more intense photon beams can somehow be obtained.

TABLE II. Expected number of events from a 60-day run at Fermilab Tevatron.

Q^2 (GeV)	y	$\frac{d^2N^{DY}}{dQ^2dy}$ (events/GeV^2)	
16	−0.6	30	$100 \leq s \leq 1200$ GeV^2
16	0.0	51	$100 \leq s \leq 1200$ GeV^2
16	0.6	29	$300 \leq s \leq 1200$ GeV^2

ACKNOWLEDGMENTS

This work was supported in part by the National Science Foundation under Grant No. NSF PHY79-00272. The authors wish to thank L. M. Jones and H. W. Wyld for helpful comments concerning theoretical matters touched upon in this work and G. Gladding and C. Olszewski for discussions concerning the feasibility of measuring small cross sections in photon beams.

APPENDIX A: PHOTON STRUCTURE FUNCTIONS — POINTLIKE CONTRIBUTIONS

The leading contributions to the QCD-renormalized contributions to the photon-parton distributions are described by functions $f_i(x)$ and $f_G(x)$ defined by Eqs. (1.1) and (1.2). We use the convenient parametrizations of Nicolaidis[26]:

$$\tfrac{1}{2}f_u(x)=x^{-1.6}(0.0036+0.28x-0.67x^2+1.5x^3-0.92x^4)\ ,$$

$$\tfrac{1}{2}f_d(x)=x^{-1.6}(0.0056+0.049x-0.125x^2+0.33x^3-0.21x^4)\ ,$$

and

$$\tfrac{1}{2}f_G(x)=8x^{-1.6}(0.021-0.033x+0.012x^2)$$

which represent well the results of more detailed calculations except for x very near 1.

APPENDIX B: PHOTON STRUCTURE FUNCTIONS — VECTOR-DOMINANCE CONTRIBUTIONS

To estimate the hadroniclike contributions to the photon structure functions we use the vector-dominance model as described by Eq. (1.3) in the text. Since the ρ^0 structure functions are themselves unknown, we must make further assumptions. Our assumptions are as follows: (1) The ρ^0 structure functions are identical to the π^0 (spin independence). (2) The momentum fractions carried separately by valence quarks, charmless sea quarks, charmed quarks, and gluons in the π^0 are the same as in the $\pi^{\pm}$. (3) The u, d, s sea components in the $\pi^{\pm,0}$ form a SU(3) flavor singlet. These assumptions together with simple isospin considerations are enough to fix the ρ^0 distributions in terms of the $\pi^{\pm}$ distributions which have been measured via $\pi^{\pm}N$ Drell-Yan production.

The above assumptions are the same as those used in Ref. 1; the resulting ρ^0 structure functions we obtain here are slightly different because we have chosen to favor the $\pi^{\pm}$ experimental results given in Ref. 13 instead than those in Ref. 14 and because we handle scale breaking by the Buras-Gaemers approximation instead of the more exact Altarelli-Parisi method.

Let $V_8^{\pi}(x,Q^2)$ be the sum of the valence-quark distributions $(u+\bar{d})$ in the π^+, $S^{\pi}(x,Q^2)$ the sum of the u, s, and d quark and antiquark sea contributions, $C^{\pi}(x,Q^2)$ the sum of the c and $\bar{c}$ quark distributions, and $G^{\pi}(x,Q^2)$ the gluon distribution in the $\pi^{\pm}$. Our model for the ρ^0 distributions can thus be written

$$u^{\rho}(x,Q^2)=\bar{u}^{\rho}(x,Q^2)=d^{\rho}(x,Q^2)=\bar{d}^{\rho}(x,Q^2)$$
$$=\tfrac{1}{4}V_8^{\pi}(x,Q^2)+\tfrac{1}{6}S^{\pi}(x,Q^2)\ , \quad \text{(B1)}$$

$$s^{\rho}(x,Q^2)=\bar{s}^{\rho}(x,Q^2)=\tfrac{1}{6}S^{\pi}(x,Q^2)\ , \quad \text{(B2)}$$

$$c^{\rho}(x,Q^2)=\bar{c}^{\rho}(x,Q^2)=\tfrac{1}{2}C^{\pi}(x,Q^2)\ , \quad \text{(B3)}$$

$$G^{\rho}(x,Q^2)=G^{\pi}(x,Q^2)\ . \quad \text{(B4)}$$

Although $\pi^{\pm}$ Drell-Yan experiments in Ref. 13 cover the range $4<Q<8.5$ GeV, most of the data fall in the interval $4<Q<5$ GeV. For simplicity we assume the experimental results to correspond to a common value, $Q_0=4$ GeV, and further that the charmed-quark contribution is negligible at this scale, $C^{\pi}(x,Q_0^2)=0$. We allow a charmed contribution to be generated at higher Q values by scale

TABLE III. Measured[a] moments of the $\pi^{\pm}$ distributions at $Q_0=4$ GeV.

n	$\langle S^{\pi}(Q_0^2)\rangle_n$	$\langle G^{\pi}(Q_0^2)\rangle_n$[b]	$\langle V_8^{\pi}(Q_0^2)\rangle_n$
2	0.100	0.550	0.350
3	0.0156	0.0859	0.148

[a]Reference 15.
[b]Constructed by assuming momentum conservation and that the gluon and sea distributions have the same x dependence at Q_0.

breaking. The gluon distribution is not probed in Drell-Yan experiments, although its $n=2$ moment can be constructed from momentum conservation. We assume the x dependence of the $G^{\pi}(x,Q_0^2)$ is the same as $S^{\pi}(x,Q_0^2)$ and are thereby able to construct completely the gluon distribution. The necessary results from the $\pi^{\pm}$ experiments are summarized in Table III.

For the valence contribution at $Q \geq Q_0$ we take

$$xV_8^{\pi}(x,Q^2)=\frac{2}{\beta(\eta_1(\bar{s}),\eta_2(\bar{s})+1)}x^{\eta_1(\bar{s})}(1-x)^{\eta_2(\bar{s})}, \tag{B5}$$

where

$$\bar{s}=\ln\left[\frac{\ln(Q^2/\Lambda^2)}{\ln(Q_0^2/\Lambda^2)}\right],$$

$$\eta_i(\bar{s})=\eta_i^0+\frac{4}{25}\eta_i'\bar{s}\ .$$

Matching the first two moments of Eq. (B5) to the experimental results given in Table III gives $\eta_1^0=0.4$, $\eta_2^0=0.9$, $\eta_1'=-0.35$, and $\eta_2'=+4.48$.

The expressions for $S(x,Q^2)$, $C(x,Q^2)$, and $G(x,Q^2)$ given in Sec. 2.2.1 of Ref. 15 are valid for any hadron under the following conditions: (1) the hadron quark distributions have been decomposed into valence, SU(3)-symmetric charmless sea, and charmed sea contributions, and (2) in regions where they are phenomenologically important the sea and gluon distributions can be determined accurately from just their first two moments. Since we have decomposed the pion distribution according to condition (1) and assumed condition (2) to be true for the pion data, we are able to parametrize $S^{\pi}(x,Q^2)$, $C^{\pi}(x,Q^2)$, and $G^{\pi}(x,Q^2)$ by the corresponding expressions in Ref. 15. The appropriate input moments for the $\pi^{\pm}$ are listed in Table III.

[1]L. M. Jones, J. D. Sullivan, D. E. Willen, and H. W. Wyld, Phys. Rev. D 20, 2749 (1979); 22, 2922(E) (1980).
[2]R. L. Jaffe, Phys. Rev. D 4, 1507 (1971).
[3]I. Kang and C. H. Llewellyn Smith, Nucl. Phys. B166, 413 (1980).
[4]A. C. Irving and D. B. Newland, Z. Phys. C 6, 27 (1980); K. Harada, Prog. Theor. Phys. 63, 982 (1980).
[5]E. Witten, Nucl. Phys. B20, 189 (1977).
[6]C. H. Llewellyn Smith, Phys. Lett. 79B, 83 (1978).
[7]R. J. DeWitt *et al.*, Phys. Rev. D 19, 2046 (1979); 20, 1751(E) (1979).
[8]W. R. Frazer and J. F. Gunion, Phys. Rev. D 20, 147 (1979).
[9]C. T. Hill and G. C. Ross, Nucl. Phys. B148, 373 (1979).
[10]W. A. Bardeen and A. J. Buras, Phys. Rev. D 20, 166 (1979).
[11]D. W. Duke and J. F. Owens, Phys. Rev. D 22, 2280 (1980).
[12]T. H. Bauer *et al.*, Rev. Mod. Phys. 50, 261 (1978).
[13]J. Badier *et al.*, in *High Energy Physics — 1980,* proceedings of the XXth International Conference, edited by L. Durand and L. G. Pondrom (AIP, New York, 1981); Phys. Lett 89B, 145 (1979).
[14]C. B. Newman *et al.*, Phys. Rev. Lett. 42, 951 (1979).
[15]A. Buras and K. Gaemers, Nucl. Phys. B132, 249 (1978).
[16]S. J. Brodsky *et al.*, Phys. Rev. Lett. 41, 672 (1978); Phys. Rev. D 19, 1418 (1979).
[17]J. Owens, Phys. Rev. D 21, 54 (1980).
[18]M. Fontannaz *et al.*, Phys. Lett. 89B, 263 (1980); Z. Phys. C 6, 241 (1980).
[19]S. D. Drell and T. -M. Yan, Phys. Rev. Lett. 25, 316 (1970).
[20]G. Altarelli, G. Parisi, and R. Petronzio, Phys. Lett 76B, 356 (1978); R. Petronzio, in *Phenomenology of Quantum Chromodynamics,* proceedings of the XIII Rencontre de Moriond, Les Arcs, France, 1978, edited by J. Trân Thanh Vân (Editions Frontieres, Gif-sur-Yvette, 1979), p. 29.
[21]K. Kajantie, J. Lindfors, and R. Raitio, Nucl. Phys. B144, 422 (1978); C. Michael and T. Weiler, in *Phenomenology of Quantum Chromodynamics* (Ref. 20), p. 179; F. Halzen and D. Scott, Phys. Rev. D 18, 3378 (1978).
[22]Y.-S. Tsai, Rev. Mod. Phys. 46, 815 (1974).
[23]G. Fox, Nucl. Phys. B131, 107 (1977).
[24]M. Levine, AEC Report No. CAR-882-25, 1971 (unpublished).
[25]G. Gladding, Fermilab 1976 Summer Study, Batavia, 1976 (unpublished), p. 309.
[26]A. Nicolaidis, Nucl. Phys. B163, 156 (1980).